

# Two-dimensional Bloch electrons in perpendicular magnetic fields: an exact calculation of the Hofstadter butterfly spectrum

S. Janecek<sup>\*,1,2,3,4</sup> M. Aichinger,<sup>3,5</sup> and E. R. Hernández<sup>1,2</sup>

<sup>1</sup>*Instituto de Ciencia de Materiales de Madrid (ICMM-CSIC), Campus de Cantoblanco, 28047 Madrid, Spain*

<sup>2</sup>*Institut de Ciència de Materials de Barcelona (ICMAB-CSIC), Campus de Bellaterra, 08193 Barcelona, Spain*

<sup>3</sup>*Johann Radon Institute for Computational and Applied Mathematics (RICAM),*

*Austrian Academy of Sciences, Altenberger Strasse 69, A-4040 Linz, Austria*

<sup>4</sup>*MathConsult GmbH, Altenberger Strasse 69, A-4040 Linz, Austria*

<sup>5</sup>*Uni Software Plus GmbH, Kreuzstrasse 15a, A-4040 Linz, Austria*

(Dated: March 11, 2013)

The problem of two-dimensional, independent electrons subject to a periodic potential and a uniform perpendicular magnetic field unveils surprisingly rich physics, as epitomized by the fractal energy spectrum known as Hofstadter's Butterfly. It has hitherto been addressed using various approximations rooted in either the strong potential or the strong field limiting cases. Here we report calculations of the full spectrum of the single-particle Schrödinger equation without further approximations. Our method is exact, up to numerical precision, for any combination of potential and uniform field strength. We first study a situation that corresponds to the strong potential limit, and compare the exact results to the predictions of a Hofstadter-like model. We then go on to analyze the evolution of the fractal spectrum from a Landau-like nearly-free electron system to the Hofstadter tight-binding limit by tuning the amplitude of the modulation potential.

The motion of electrons in a crystalline solid subject to a magnetic field has been considered since the early days of quantum mechanics [1]. The field splits the crystal's electronic bands into sub-bands and internal mini-gaps; the energetic arrangement of these sub-bands forms a fractal structure reminiscent of a butterfly when plotted as a function of the field [8]. Significant experimental effort has been devoted to detecting signatures of this energy spectrum in two-dimensional electron gases (2DEGs) [2, 3]. For independent electrons, the situation is described by the single-particle Schrödinger equation,

$$H\psi(\mathbf{r}) \equiv \left[ \frac{1}{2m}\Pi^2 + V(\mathbf{r}) \right] \psi(\mathbf{r}) = E\psi(\mathbf{r}), \quad (1)$$

where  $H$  is the Hamiltonian,  $\psi(\mathbf{r})$  is an eigenstate with energy  $E$ ,  $\Pi = \mathbf{p} + e\mathbf{A}(\mathbf{r})$  is the dynamical momentum operator and  $\mathbf{A}(\mathbf{r})$  is the vector potential corresponding to the magnetic field,  $\mathbf{B} = \nabla \times \mathbf{A}$ . We take the field to be uniform and oriented along the  $z$ -direction,  $\mathbf{B} = B\mathbf{e}_z$ . The electrons are restricted to the two-dimensional (2D)  $xy$ -plane, and the external potential  $V(\mathbf{r})$  is periodic on a Bravais lattice defined by vectors

$$\mathbf{R}_{\mathbf{n}} = j\mathbf{a} + k\mathbf{b}, \quad \mathbf{n} = (j, k) \in \mathbb{Z}^2. \quad (2)$$

To date, this problem has been chiefly approached by approximations starting from two complementary limits, considering either the influence of a weak magnetic field on the band structure resulting from a strongly varying potential  $V(\mathbf{r})$  [4, 5], or the influence of a small modulation potential on the Landau-quantized electrons in a strong field [5, 6]. In the strong potential limit, one typically starts with a tight-binding (TB) approximation for a single band of the zero-field ( $\mathbf{A} = 0$ ) problem,  $E(\mathbf{k})$ , where  $\mathbf{k}$  is the crystal momentum. Then,

an effective Hamiltonian for the magnetic field problem is generated from  $E(\mathbf{k})$  through the Peierls substitution  $\mathbf{k} \rightarrow (\mathbf{p} + e\mathbf{A})/\hbar$  [1, 7]. This procedure was used, among others, by Hofstadter in his seminal article for a nearest-neighbor (NN) TB model of the 2D square lattice [8]. There are a number of simplifications inherent to this approach: (i) the TB approximation of the zero-field band structure, (ii) the restriction to electrons in a single band, (iii) the neglect of the diamagnetic energy of the TB orbitals and the field dependence of the TB hopping integrals. This has been shown to lead to quantitative as well as qualitative errors for both nearly free and tightly bound two-dimensional electrons [9–12]. Generalization of the effective Hamiltonian approach has turned out to be difficult, see, e.g., Ref. [13]. Surprisingly, the strong field approach is closely related to the strong potential one: if potential-induced coupling between different Landau levels is neglected, the same secular equation results, but with the magnetic field replaced by its inverse [5]. Including such coupling has a profound effect on the calculated energy spectrum [14, 15], even for weak coupling strength. The resulting rearrangement of the Hofstadter butterfly has recently been confirmed by experiments [3]; we take this as a strong indication that experiments can only be fully understood by going beyond the approximate schemes described above.

*Method.* In the absence of magnetic field, Bloch's theorem, which results from the commutation of the lattice translations with the Hamiltonian, allows to restrict the calculation of the eigenfunctions  $\psi(\mathbf{r})$  to one primitive cell of the lattice in Eq. (2). As these translations do not leave the vector potential  $\mathbf{A}(\mathbf{r})$  invariant, they no longer commute with  $H$  when a magnetic field is present; consequently, the eigenfunctions  $\psi(\mathbf{r})$  are not Bloch waves.

By combining a lattice translation with a suitable gauge transformation to counteract its effect upon the vector potential, one can define *magnetic translation operators*,  $T_A(\mathbf{R}_n)$ , that do commute with  $H$ , see Refs. [16–18]. The operators  $T_A(\mathbf{R}_n)$  do not, however, form a group. For a rational field, where the number of magnetic flux quanta per unit cell,  $\alpha = \frac{1}{2\pi} \frac{e}{\hbar} (\mathbf{a} \times \mathbf{b}) B$ , is a rational number,  $\alpha = p/q$  with  $p$  and  $q$  relative prime, one can choose a larger magnetic lattice that has an integer number of  $p$  flux quanta passing through each cell, e.g.,

$$\mathbf{S}_n = j\mathbf{a} + k(q\mathbf{b}), \quad \mathbf{n} = (j, k) \in \mathbb{Z}^2. \quad (3)$$

On this lattice, a generalized version of the Bloch theorem holds [18]: for an orthorhombic lattice and Landau gauge,  $\mathbf{A}(\mathbf{r}) = Bx\mathbf{e}_y$ , the solutions of Eq. (1) can be chosen of the form  $\phi(\mathbf{r}) \equiv e^{i\boldsymbol{\theta}\mathbf{r}} u^{\boldsymbol{\theta}}(\mathbf{r})$ , where  $u^{\boldsymbol{\theta}}(\mathbf{r})$  obeys

$$u^{\boldsymbol{\theta}}(\mathbf{r} + \mathbf{S}) = \exp \left[ -i \frac{e}{\hbar} B S_{xy} \right] u^{\boldsymbol{\theta}}(\mathbf{r}), \quad (4)$$

and the magnetic crystal momentum  $\boldsymbol{\theta}$  is restricted to the first Brillouin zone of (3). This condition allows to restrict the calculation of  $u^{\boldsymbol{\theta}}(\mathbf{r})$  to one primitive cell of the magnetic lattice. The functions  $u^{\boldsymbol{\theta}}(\mathbf{r})$  exhibit a peculiar topology in a space where their  $y$ -component is expanded in a Fourier series, see Ref. [19]. This allows to take into account the boundary condition (4) in a natural way when the diffusion method is used for solving the Schrödinger equation [20, 21]. We have summarized the steps leading to Eq. (4) and the technical details of the diffusion method in the Supplementary Information.

At a fixed rational field,  $\alpha = p/q$ , we obtain the bands  $E_j(\boldsymbol{\theta})$  by numerically solving Eq. (1) for a grid of  $\boldsymbol{\theta}$ -values spanning the magnetic Brillouin zone (MBZ) corresponding to this field. The density of states (DOS) as a function of the field,  $\rho(B, E)$ , can then be calculated by integrating the bands over the MBZ and repeating the process for different fields. The rational field can only be tuned in discrete steps,  $\alpha_P = P/Q$ , where  $P, Q \in \mathbb{Z}$ . The size of the magnetic unit cell depends on the reduction of  $P/Q$  to a quotient of relatively prime integers  $p/q$ , and is  $q$  times as large as the zero-field (“geometric”) unit cell. At the field  $\alpha_P$ , one zero-field band is thus expected to split into  $q$  magnetic bands, which are known to cluster in groups of  $p$  bands [8]. The pattern of distinct prime factors of  $P$  and  $Q$  as  $\alpha_P$  is swept across a range of fields gives rise to the self-similar, fractal pattern of gaps in the DOS that has become known as the Hofstadter butterfly.

When the Fermi energy of the system lies in a gap, i.e., a region where  $\rho(B, E_F)$  is zero, the Hall conductance  $\sigma_{xy}$  assumes a quantized value,  $\sigma_{xy}^{\text{gap}} = ne^2/h, n \in \mathbb{Z}$ . The fundamental topological reason for this quantization was revealed by Thouless *et al.* [22], who showed that both in the strong field and strong potential limits the Kubo-Greenwood formula for  $\sigma_{xy}$  is related to the Chern number of the  $U(1)$  bundle over the magnetic Brillouin zone. This was later argued [23] to be a direct consequence of

the magnetic translation symmetry, Eq. (4). Sweeping either the magnetic field or the Fermi energy through the fractal pattern of minigaps inside a broadened band or Landau level results in a peculiar, non-monotonous Hall effect [22]. Indications of this behavior have been found in experiments [2]. In this work we have used an alternative approach, introduced by Středa [24], to obtain  $\sigma_{xy}^{\text{gap}}$  from the numerically calculated DOS,

$$\sigma_{xy}^{\text{gap}}(B, E_F) = e \frac{\partial \rho(B, E')}{\partial B} \Big|_{E'=E_F}. \quad (5)$$

In our numerical calculations, we have studied a simple system consisting of a two-dimensional square lattice of potential wells with the symmetrized Fermi function form [25],

$$V(r) = U \coth \left( \frac{r_0}{2d} \right) \frac{\sinh \left( \frac{r_0}{d} \right)}{\cosh \left( \frac{r}{d} \right) + \cosh \left( \frac{r_0}{d} \right)}, \quad (6)$$

with parameters

$$r_0 = 39.7 \text{ nm}, \quad d = 1.59 \text{ nm}, \quad a = 100 \text{ nm}, \quad (7)$$

where  $a$  is the lattice spacing. The potential is illustrated in Fig. (1a); the parameters are set to loosely reproduce the conditions of earlier experimental studies [2, 3].

*Strong Potential Regime.* We first compare the spectrum generated by the full Schrödinger equation (1) to the results of a TB approximation similar to the one used by Hofstadter. We thus choose a fairly deep modulation potential,

$$U = -V_0 \equiv -8.4 \text{ meV}. \quad (8)$$

We obtained the band structure and DOS at zero magnetic field [see Fig. (1c)] by numerically solving the corresponding single-particle Schrödinger equation. We then fitted a TB model to the lowest three bands [black dashed lines in Fig. (1c)], and employed the Peierls substitution to obtain the fractal energy spectra shown in Fig. (1d), see the Supplementary Information for details. The lowest band [ $n = 1$  in Fig. (1c)] required only nearest-neighbor hopping integrals in the TB band model for an adequate fit, and thus yields a spectrum corresponding to that obtained by Hofstadter [8] [left panel of Fig. (1d)]. The second and third bands required up to 3<sup>rd</sup>-nearest-neighbor hoppings, which lead to significantly distorted versions of Hofstadter’s butterfly, shown for the second band on the right panel of Fig. (1d). The spectrum of the third band is similar and is not shown. Our findings qualitatively agree with the results of Ref. [26].

In Fig. (2a) we show the energy spectrum of the six lowest bands, as obtained by numerically solving the full magnetic eigenvalue problem, Eq. (1), using the scheme outlined above. A maximum magnetic unit cell size of  $Q = 32$  was employed in the calculation. For comparison, the spectrum of an isolated potential well is plotted

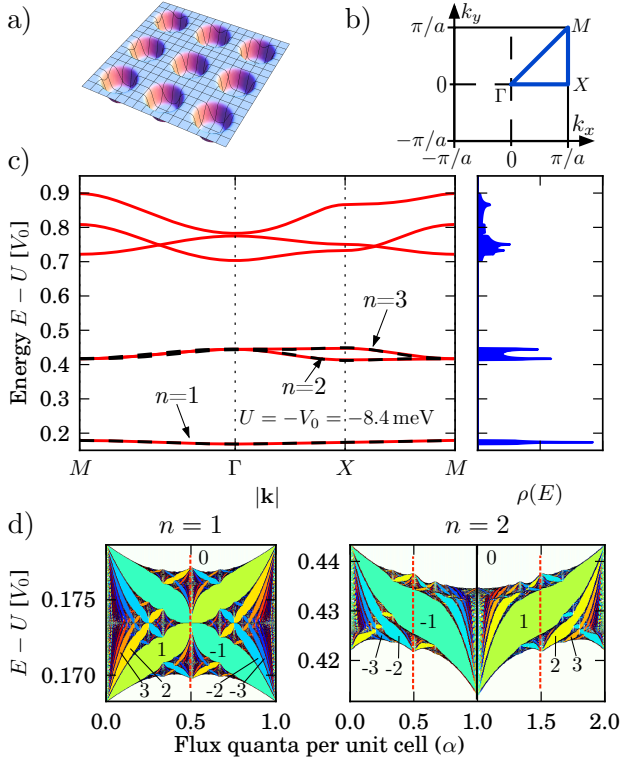


FIG. 1: (color online). a) Schematic plot of the periodic Fermi well potential. b) First Brillouin zone of the reciprocal lattice. c) *Left panel*: Zero-field band structure of the potential with parameters (7) and  $U = -V_0$ . Solid red lines show bands obtained by numerically solving the Schrödinger equation, dashed black lines are TB bands fitted to these exact bands (see text). *Right panel*: DOS  $\rho(E)$  obtained from the full Schrödinger equation. d) Hofstadter butterflies for the two lowest bands. Areas with non-zero DOS are printed black, and the gaps are colored according to the corresponding quantized Hall conductance  $\sigma_{xy}^{\text{gap}}$  in units of  $e^2/h$ . White indicates zero Hall conductance, warm (cold) colors indicate positive (negative) Hall conductance. A number of larger gaps are labeled with the corresponding Hall conductance for reference. The butterflies are periodic in the flux, one period being shown in each case.

in Fig. (2c). It bears a strong resemblance to the Fock-Darwin (FD) spectrum [27] of a parabolic well, we will thus refer to these states as “FD states” in the following. It can be seen in Fig. (2a) that in the periodic system the FD states of the isolated well are broadened into bands with a fractal internal structure that is qualitatively well described by the Hofstadter butterfly. In the exact result the periodicity of the Hofstadter spectrum is superimposed onto the field dependence of the corresponding FD state; this field-dependence is not taken into account in the TB model with constant hopping integrals. In general, higher energy levels, having more extended wave functions, undergo larger broadening at a given flux value. Conversely, bands become narrower with increasing field, as their wave functions become more spatially

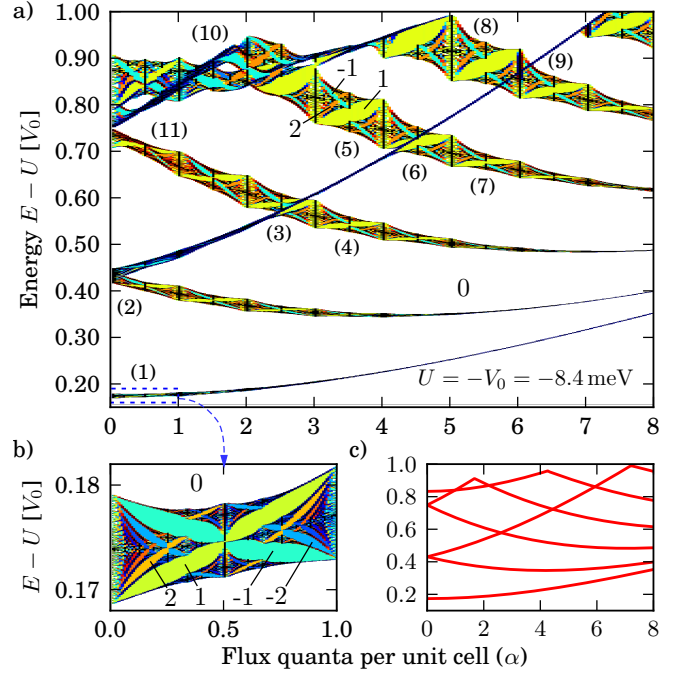


FIG. 2: (color online). Magnetic energy spectrum (DOS and Hall conductance  $\sigma_{xy}^{\text{gap}}$ ) for the lowest six bands of the square Fermi well lattice with parameters (7) and  $U = -V_0$ , calculated by numerically solving Eq. (1). The color coding and labeling is as in Fig. (1). Panel (b) shows a magnified portion of the lowest band indicated by the dashed box in panel (a). Panel (c) shows the energy spectrum of an isolated Fermi well potential, Eq. (6). It strongly resembles the spectrum of a parabolic potential (the Fock-Darwin spectrum [27]).

localized, tending to Landau levels in the limit of high field intensities. In the TB model, the main effect of increasing the second- and third-nearest neighbor hoppings is a distortion of the butterfly that opens a gap at flux strengths of  $\alpha_j = j + 1/2$ , with  $j \in \mathbb{Z}$ , indicated by the vertical (red) dotted lines in the butterflies in Fig. (1d). This behavior is also present in the exact results, compare regions (4)–(5) or (7)–(8) in Fig. (2a). The gap widens for higher-energy bands, consistent with the TB approximation, where such bands need to be modeled by larger hopping integrals to more distant neighbors. The gap decreases again with increasing field due to the stronger localization of the wave functions, an effect that is not included in the TB description with  $B$ -independent hopping. Band crossings, which are not described within the single-band Peierls approximation, are an interesting subject for future studies: the narrow third FD band seems to disrupt the butterfly pattern of the broader bands it crosses in regions (3) and (6), but does not seem to exert any noticeable effect in region (9). At higher energies [see region (10)], where multiple bands cross, the resulting fractal spectrum can assume a form that is very different from the original Hofstadter butterfly.

*Intermediate Potential Regime.* We now explore the evolution of the spectrum as the potential is changed from nearly flat (strong field limit) to highly modulated (strong potential limit). The intermediate stages of this evolution are not accessible to the approximate methodologies hitherto employed. We use the square lattice potential with the parameters given in Eq. (7), but change the well depth  $U$ . We start with a very shallow potential ( $U = -0.06 V_0$ ), which corresponds to a Landau-like system with nearly-free electrons in a magnetic field. The resulting spectrum is illustrated in Fig. (3a); it exhibits the typical “Landau fan” form, with slightly broadened Landau levels (LLs) that display an internal fractal structure of minigaps (most evident in the lowest level,  $L_0$ ). The Hall conductance between LLs increases monotonically in steps of  $e^2/h$ , consistently with the integer quantum Hall effect. Furthermore, an emerging white gap ( $\sigma_{xy}^{\text{gap}} = 0$ ) can be observed at low field ( $\alpha = 0 - 1$ ,  $E \approx 0.11 V_0$ ). When the potential modulation is increased to  $U = -0.13 V_0$  [Fig. (3b)] this gap is seen to widen further, practically cutting off a low-energy triangular section (marked “T” in the figure) from all LLs  $L_n$  with  $n > 0$ . At  $\alpha = 1$  the upper-right tip of this triangular cluster of states retains a tenuous link to the broadened  $L_1$  Landau band, at the position indicated by the blue arrow. At the same time, the minigaps at  $\alpha \geq 1$  in the lowest Landau band  $L_0$  have broadened further, to the point where the band is only held together by a narrow sub-band at  $\alpha = 1$ , indicated by the red arrow. The Hall conductance in the gap between  $L_0$  and  $L_1$  at  $\alpha = 1$  is still  $\sigma_{xy}^{\text{gap}} = 1$ . But upon further increasing the modulation strength, the gap first closes and then reopens with the above links reversed: at  $U = -0.26 V_0$  [Fig. (3c)], the tip of the triangular cluster is now connected to the lowest miniband of  $L_0$  (blue arrow), while the rest of the  $L_0$  miniband is connected to  $L_1$  (red arrow). At the same time, the gap has changed its character to  $\sigma_{xy}^{\text{gap}} = 0$ , resulting in the first clearly discernible FD-like band  $F_0$ , separated from all higher energy states by an unbroken white gap. Most of  $F_0$  is formed from the lowest miniband of the LL  $L_0$ , except for the triangular cluster of states in  $\alpha < 1$ , which originates from higher LLs. The process of formation of the first FD band ( $F_0$ ) that is incipient at  $\alpha = 1$  in Fig. (3b) can be seen to repeat itself at  $\alpha = 2$  for the second FD band ( $F_1$ ) [Fig. (3c), green and purple arrows] and at  $\alpha = 3$  for the third FD band ( $F_2$ ) [Fig. (3d)]. The gradual transformation from LLs to FD-like bands thus proceeds by the re-connection of minibands from one broadened LL to those of neighboring LLs. This rearrangement process fragments the large triangular gaps between LLs in the weak potential limit into minigaps encapsulated by the emerging FD-like bands. As a result, the FD states  $F_0, F_1, F_2$  in Fig. 3d are composed of a low-field section that originates from higher LLs (triangle T in case of  $F_0$ , one Hofstadter butterfly segment plus a triangular cluster in case of  $F_1$ ,

etc.), and a high-field section that is one miniband of the lowest LL  $L_0$ .

The above results show that with the method presented here it is possible to perform exact calculations of the spectrum of independent electrons in a 2D periodic potential and constant perpendicular magnetic field. The same technique is readily applicable to solve the Kohn-Sham equations of density functional theory (DFT) which are expected to provide a reasonable description at least for weakly correlated electron systems. Experimental techniques have recently become available to directly probe the local DOS in 2DEGs on surfaces in a perpendicular magnetic field using scanning tunneling spectroscopy, making possible the detection of spatial features of some LLs [32], and even measuring their response to a 1D periodic potential due to surface buckling [33]. Such developments may presently bring about additional possibilities of experimentally determining the spectral features of the 2DEG subject simultaneously to a periodic potential and a perpendicular magnetic field, contrasting them with the predictions reported herein. The Hofstadter butterfly is not unique to the system discussed here. The basic principle underlying the fractal energy spectrum is the presence of two competing symmetries (in the case studied here, the periodicity of the lattice and the symmetry of the Landau orbits, which is governed by the area required by one magnetic flux quantum). Similar patterns have been observed or predicted to occur in a variety of very different systems, such as microwaves transmitted through a waveguide with a periodic arrangement of scatterers [28], the electronic [29] and vibrational [30] spectra of incommensurate crystals, ultracold atoms in optical lattices [31], and photonic crystals [34, 35]. The topological protection of the quantum Hall phase has been shown to improve the performance of optical delay lines and to overcome limitations related to disorder in photonic technologies [35]. We hope that the method presented here will also prove beneficial in these related fields.

We wish to thank A. García and E. Krotscheck for helpful discussions. SJ was funded by the Austrian Science fund FWF under project no. J2936-N, E.R.H. by the Spanish Ministry of Science and Innovation through project FIS2009-12721-C04-03. SJ would like to thank ICMAB and ICM for their hospitality during his stay. We acknowledge CESGA and the Johannes Kepler University Linz for the use of their computer facilities, where the results reported here were obtained.

- 
- [1] R. Peierls, Z. Physik **80**, 763 (1933).
  - [2] C. Albrecht, J. Smet, K. von Klitzing, D. Weiss, V. Umansky, and H. Schweizer, Phys Rev Lett **86**, 147 (2001).
  - [3] M. Geisler, J. Smet, V. Umansky, K. von Klitzing,

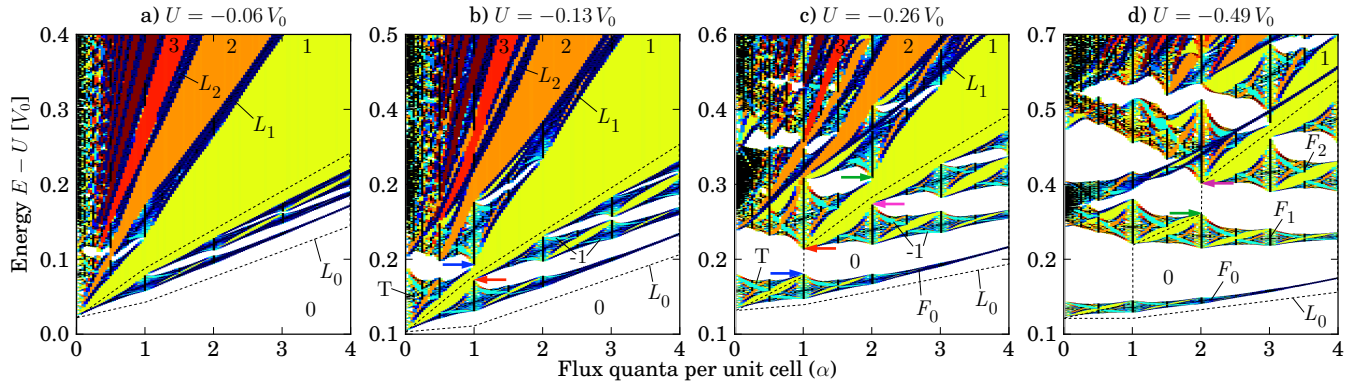


FIG. 3: (color online). Energy spectra for different strengths of the modulation potential, ranging from a “Landau-like” system of nearly free electrons [ $U = -0.06 V_0$ , panel a)] to a moderately deep potential [ $U = -0.49 V_0$ , panel d)] already resulting in a “Fock-Darwin”-like spectrum. Energies and modulation potentials  $U$  are given in units of  $V_0$ , the depth of the modulation potential used to generate Fig. 2. Gaps are color coded and labeled with their corresponding Hall conductance as in Fig. 1. Landau levels are denoted by  $L_1, L_2, \dots$ , Fock-Darwin-like states  $F_0, F_1, \dots$ . The dotted line encloses the broadened lowest Landau level. The label “T” indicates the triangular cluster of states referenced in the text.

- B. Naundorf, R. Ketzmerick, and H. Schweizer, *Phys Rev Lett* **92**, 256801 (2004).
- [4] P. Harper, *P Phys Soc Lond A* **68**, 874 (1955).
- [5] D. Langbein, *Phys Rev* **180**, 633 (1969).
- [6] G. Wannier, G. Obermair, and R. Ray, *Phys Status Solidi B* **93**, 337 (1979).
- [7] J. Luttinger, *Phys Rev* **84**, 814 (1951).
- [8] D. Hofstadter, *Phys Rev B* **14**, 2239 (1976).
- [9] Y. Hasegawa, P. Lederer, T. Rice, and P. Wiegmann, *Phys Rev Lett* **63**, 907 (1989).
- [10] V. Nicopoulos and S. Trugman, *Phys Rev Lett* **64**, 237 (1990).
- [11] A. Alexandrov and H. Capellmann, *Phys Rev Lett* **66**, 365 (1991).
- [12] G. Vugalter and A. Pastukhov, *J Phys A-Math Gen* **37**, 5763 (2004).
- [13] W. Kohn, *Phys Rev* **115**, 1460 (1959).
- [14] D. Springsguth, R. Ketzmerick, and T. Geisel, *Phys Rev B* **56**, 2036 (1997).
- [15] O. Kühn, V. Fessatidis, H. Cui, P. Selbmann, and N. Horning, *Phys Rev B* **47**, 13019 (1993).
- [16] E. Brown, *Phys Rev A-Gen Phys* **133**, 1038 (1964).
- [17] J. Zak, *Phys Rev A-Gen Phys* **134**, 1607 (1964).
- [18] H. J. Fischbeck, *Phys Status Solidi* **38**, 11 (1970).
- [19] W. Cai and G. A. Galli, *Phys. Rev. Lett.* **92**, 186402 (2004).
- [20] S. A. Chin, S. Janecek and E. Krotscheck., *Chem. Phys. Lett.* **470**, 342–346 (2009).
- [21] M. Aichinger, S. A. Chin and E. Krotscheck, *Comp. Phys. Comm.* **171**, 197–207 (2005).
- [22] D. Thouless, M. Kohmoto, M. Nightingale, and M. Denijs, *Phys Rev Lett* **49**, 405 (1982).
- [23] I. Dana, J. E. Avron, and J. Zak, *J Phys C Solid State* **18**, L679 (1985).
- [24] P. Streda, *J Phys C Solid State* **15**, L717 (1982).
- [25] D. Sprung and J. Martorell, *J Phys A-Math Gen* **30**, 6525 (1997).
- [26] F. Claro, *Phys Status Solidi B* **104**, K31 (1981).
- [27] C. G. Darwin, *Proc. Camb. Phil. Soc.* **27**, 86 (1930).
- [28] U. Kuhl and H. Stockmann, *Phys Rev Lett* **80**, 3232 (1998).
- [29] C. de Lange and T. Janssen, *Phys Rev B* **28**, 195 (1983).
- [30] M. Quilichini and T. Janssen, *Rev Mod Phys* **69**, 277 (1997).
- [31] D. Jaksch and P. Zoller, *New J Phys* **5**, 56 (2003).
- [32] K. Hashimoto *et al.*, *Phys. Rev. Lett.* **109**, 116805 (2012).
- [33] Y. Okada *et al.*, *Phys. Rev. Lett.* **109**, 166407 (2012).
- [34] K. Fang, Z. Yu and S. Fan *Nature Photonics* **6**, 782 (2012).
- [35] M. Hafezi, E. A. Demler, M. D. Lukin and J. M. Taylor *Nature Phys.* **7**, 907 (2011).